Marine Geodesy
Publication details, including instructions for authors and subscription information:
http://www.tandfonline.com/loi/umgd20

Calibration/Validation of an Altimeter Wave Period Model and Application to TOPEX/Poseidon and Jason-1 Altimeters

Y. QUILFEN [a] , B. CHAPRON [a] , F. COLLARD [b] & M. SERRE [c]
[a] Institut Français de Recherche pour l'Exploitation de la Mer Brest, France
[b] BOOST Technologies Brest, France
[c] University of North Carolina, Chapel Hill, North Carolina, USA

Available online: 12 Aug 2010

To cite this article: Y. QUILFEN, B. CHAPRON, F. COLLARD & M. SERRE (2004): Calibration/Validation of an Altimeter Wave Period Model and Application to TOPEX/Poseidon and Jason-1 Altimeters, Marine Geodesy, 27:3-4, 535-549

To link to this article: http://dx.doi.org/10.1080/01490410490902025

Marine Geodesy, 27: 535–549, 2004

ISSN: 0149-0419 print / 1521-060X online
DOI: 10.1080/01490410490902025

Taylor & Francis
Taylor & Francis Group

Calibration/Validation of an Altimeter Wave Period Model and Application to TOPEX/Poseidon and Jason-1 Altimeters

Y. QUILFEN
B. CHAPRON

Institut Français de Recherche pour l'Exploitation
de la Mer
Brest, France

F. COLLARD

BOOST Technologies
Brest, France

M. SERRE

University of North Carolina
Chapel Hill, North Carolina, USA

The altimeter radar backscatter cross-section is known to be related to the ocean surface wave mean square slope statistics, linked to the mean surface acceleration variance according to the surface wave dispersion relationship. Since altimeter measurements also provide significant wave height estimates, the precedent reasoning was used to derive empirical altimeter wave period models by combining both significant wave height and radar backscatter cross-section measurements. This article follows such attempts to propose new algorithms to derive an altimeter mean wave period parameter using neural networks method. Two versions depending on the required inputs are presented. The first one makes use of Ku-band measurements only as done in previous studies, and the second one exploits the dual-frequency capability of modern altimeters to better account for local environmental conditions. Comparison with in situ measurements show high correlations which give confidence in the derived altimeter wave period parameter. It is further shown that improved mean wave characteristics can be obtained at global and local scales by using an objective interpolation scheme to handle relatively coarse altimeter sampling and that TOPEX/Poseidon and Jason-1 altimeters can be merged to provide altimeter mean wave period fields with a better resolution. Finally, altimeter mean wave period estimates are compared with the WaveWatch-III numerical wave model to illustrate their usefulness for wave models tuning and validation.

Keywords altimeter, wave period, neural network, wave model

Sea state can be described in numerous ways, from a near complete spectral description as deduced from buoys, airborne or spaceborne RAR/SAR instruments, to rough visual estimates as provided by ships of opportunity. It is also often practical and accurate enough

Received 30 May 2004; accepted 16 September 2004.
Address correspondence to Y. Quilfen, Space Oceanography Laboratory, IFREMER, BP70, Plouzané, France. E-mail: yves.quilfen@ifremer.fr

to describe the local sea state using integrated quantities (e.g., significant wave height (Hs), mean ocean wave period, and wave steepness). The former two parameters can be obtained from ocean wave spectral moments of buoy. For altimeter measurements, significant wave height estimates are easily obtained and are currently being assimilated in numerical wave models. These Hs can be complemented by an "altimeter mean wave period" derived from the combination between Hs and the backscatter coefficient, also referenced as the normalized radar cross-section (NRCS) (Davies et al. 1997; Hwang et al. 1998; Gommenginger 2003), to give a more complete description of the sea-state. The recent algorithm proposed by Gommenginger (2003) shows a good agreement when compared with buoy measurements but leaves residual dependencies of the retrieved altimeter mean wave period parameter as a function of the sea-state maturity.

Hereafter, an empirical algorithm is proposed using neural networks to fully exploit the altimeter capability to provide regional and global characteristics of the wave field. The approach is based upon neural network modelization and will exploit the dual-frequency characteristics of the TOPEX/Poseidon and Jason-1 altimeters. Indeed, it is anticipated that the C-band measurements shall better filter out the shorter sea surface scales to be closer to buoy measurements whose shorter sampled waves are gravity waves. The use of the information contained in the difference between C and Ku band radar cross sections, together with the wind speed, shall better constrain the wind sea contribution in the retrieved parameter.

The next section presents the current altimeter mean wave period models and the two new neural models. In this section, the neural network methodology and the data used to derive the neural models are also described. Then a section is devoted to the validation of the neural models and to their comparison with the SOC model. Since the neural models have been defined with the T/P data, a cross-calibration with Jason-1 measurements is performed in this section. In the next section, a mapping of the mean altimeter wave period is provided to illustrate the opportunity of the T/P and Jason-1 tandem mission to provide new sea state information at global and local scales. A comparison with the numerical model WaveWatch-III (Tolman et al. 2002) is done in the final section to illustrate the interest of the altimeter mean wave period to validate and tune the numerical wave models.

The Altimeter Wave Period Models

Generality

Ideally, for a wind sea condition, the ocean surface will rapidly roughen. With time or fetch, the sea develops and using similarity laws (e.g., Kitaigorodskii 1973), high correlation between nondimensional wind sea energy and inverse wave age are expected. Consequently, estimating the wind and the significant wave height shall be sufficient to infer the wave period. On the other hand, considering the possible direct inverse relationship between altimeter NRCS and mean surface slope variance (Barrick 1974), the dispersion relationship can also be invoked to derive an altimeter-integrated mean wave period by using simultaneous altimeter significant wave height and NRCS measurements as $Talt \propto Hs^2\sigma^{1/4}$ (Gommenginger et al. 2003). Finally, globally distributed crossovers of altimeter and scatterometer observations have clearly demonstrated that ocean altimeter backscatter correlates with both the near surface wind speed and the sea state (Gourrion et al. 2002a). Especially considering C-band measurements, Gourrion et al. (2002b) further demonstrated excellent correlation between buoy acceleration variance estimates and inferred C-band mean square surface slopes.

Based on such reasoning and observations, enhanced use of altimeter observations to infer sea state degree of development and/or mean period/wavelength is proposed. A few

wave period models have been reported in the scientific literature (i.e., Davies et al. 1997; Hwang et al. 1998; Gommenginger et al. 2003). The last, developed at the Southampton Oceanographic Center (SOC), hereafter referenced as the SOC model, has been shown to be a substantial improvement compared to the former ones. It will thus be used as a reference for comparison with the neural models presented here. As outlined above, simple relationship considerations enable relating the ocean waves period to the altimeter significant wave height (Hs) and normalized radar cross-section (NRCS), as done empirically in the SOC model by using the T/P Ku band measurements. However, weight and exponent choices to build an empirical formulation such as the SOC model may be complicated, and so we use a well-trained neural model to help build our algorithm without having to define a priori values for weights and exponents. As a first step, and to be used later as a reference and in comparison with the SOC model, we have developed a first neural model, called NN-1, solely using as inputs the Ku-band Hs and NRCS parameters. Ku band measurements were used in the past because the first models were developed for single frequency altimeter like Geosat. Today's altimeters are dual-frequency sensors (T/P, Jason-1, ENVISAT) and offer an opportunity to exploit these capabilities. Indeed, the buoy and altimeters are sensitive to different sea surface scales. The altimeter measurements are closely related to short scales (down to centimetric) while the buoy measurements are sensitive to gravity waves longer than 10 m. The additional use of the T/P C-band measurements less sensitive to the shorter scales, combined with the Ku-band ones in the neural model to retrieve the mean wave period, will provide significant reduction of the mismatch between the buoy and altimeter measurements. Altimeter measurements also exhibit a variability associated with the sea state maturity (Glazman and Pilorz 1990; Fu and Glazman 1991), leading to a bias in the retrieved altimeter mean wave period if not accounted for. Information on sea state maturity requires additional knowledge of the surface wind speed. Wind speed and C-band backscatter coefficient will, therefore, be used to constrain a second neural model, NN-2, that will depend on four altimeter parameters: Hs at Ku band, NRCS at Ku and C bands, and the 10 m surface wind speed.

Calibration of altimeter wave period models requires reference measurements of the mean wave period. This is usually provided by buoys but different computations of the mean wave period can be done from the buoy wave spectrum. There is no conclusive proof or evidence about which one is the best or the "usual" one to use. In this study we have used the mean wave period parameter provided in the NDBC archive defined as $T = \sqrt{m_0/m_2}$, where m_0 and m_2 are the zero and second order moments of the measured wave spectrum. As defined, T is a zero crossing period corresponding to the time between two successive crossings of the mean sea level.

Data

The analyses are based upon a set of TOPEX/Poseidon (T/P) altimeter measurements collocated with the National Data Buoy Center (NDBC) buoys. The T/P Geophysical Data Records (GDR) are processed by the AVISO center, and the collocation with the NDBC buoys was performed at Centre ERS d'Archivage et de Traitement (CERSAT). The NDBC data have been collected over the period from October 1992 to March 2002 by 33 buoys. These buoy measurements are converted to 10-meter neutral winds, using a log-profile relation accounting for the atmospheric stability. The buoy one-hour average estimate the closest to the time of T/P satellite overpass is collocated with the altimeter data. The separation distance between measurements is less than 25 km. A data screening is applied with the following criteria: the buoy mooring depth is greater than 50 m; the buoy wind speed is in the range 0–25 m/s. For altimeter measurements, those during which rain occured are

filtered using both the rain flag in the GDRs and the Tournadre and Morland algorithm (1997). An upper threshold of 16 dB and 20 dB has been applied for the Ku and the C band backscatter coefficient, respectively. Measurements beyond these thresholds are considered as outliers, since they are likely to correspond to surface slicks for which there are no surface waves. The thresholds have been determined after a careful data screening. With the above data editing, 6679 collocated data pairs have been compiled. This dataset corresponds to a broad range of wind and sea situation thanks to a fairly wide spread buoy network, covering the North American coasts, the gulfs of Alaska and Mexico, and the Hawai Islands area.

Neural Network Architecture and Training Process

The main advantage of using neural networks to define an altimeter mean wave period model is that it does not require an a priori knowledge of the mathematical relation linking the different variables. The neural model definition requires the identification of the pertinent variables and the determination of the network architecture adapted to the input variables set. We use a neural network modelization in the form of a multilayer perceptron network (Hornik et al. 1989; White 1990). The selected network architecture has been designed to enable the reproduction of a family of functions already used in previous parametric models definition. In particular, the first layer transfer function is an exponential to account for the multiplicative relationships between the significant wave height and the normalized backscatter cross-section inputs. The other layers are composed of linear transfer functions to avoid saturation effects near the low and high ends of the wave period range where training dataset density is low. The training process, based on feedforward gradient back propagation technique, is looking for an optimal set of network parameters in an iterative scheme that minimizes the mean square difference between the predicted and observed mean wave period. We make use of the Levenberg-Marquardt gradient descending technique to search for this minimum, starting from a random set of network parameters. A data normalization process is performed by scaling and centering the data before entering the neural training process. The training dataset is selected within the global dataset by randomly extracting no more than a maximum number of data per interval of the output parameter. This maximum number was set at 40 samples in each data bin of 0.5 seconds. With these criteria, 775 measurements are randomly selected for the training data set. The training process is performed using this subsample of the buoy wave period dataset and the corresponding altimeter measurements. The training process is repeated 100 times with different training datasets randomly selected in order to find the neural network for which we obtain the better fit between the buoy wave period distribution and the altimeter wave period distribution over the global dataset. Since the obtained neural model has been derived using a subset of the data, the network performance evaluation is performed using the remaining part of the dataset.

After the training process we obtain the following formulation for the two neural models NN-1 and NN-2:

$$tnn_1 = e^{-17.1642\times a+13.5844}, \tag{1}$$

where

$$a = \frac{1}{1+e^{0.6573\times Hs^{0.1084}\times\sigma_{Ku}^{0.2962}-2.2377}}, \quad \text{and} \quad tnn_2 = e^{5.7474-1.4688\times a+1.7943\times b}, \tag{2}$$

where

$$a = \frac{\sigma_{Ku}^{0.3082}}{\sigma_C^{0.2352} \times Hs^{0.0981}} \times e^{1.5068 \times b}, \quad \text{and} \quad b = \frac{2}{1 + e^{-1.8612 - 0.08 \times U_{10}}} - 1.$$

In these equations σ_{Ku} and σ_C are the altimeter normalized radar cross-sections in dB at Ku-band and C-band, respectively; Hs is the significant wave height; and U_{10} is the 10 m surface wind speed computed with the Gourrion et al. algorithm (2002a).

Results

Wave Period Models Validation

Comparisons of the SOC and the neural models with the mean buoy wave period are illustrated in Figures 1 and 2 and Tables 1 to 3. An overall improvement is obtained with the neural models, as portrayed on Figure 1. The comparison between the buoy and the T/P altimeter wave period measurements is color-coded as a function of the inverse wave age computed as $U/Cp \propto U/Tp$, where U is the buoy wind speed and Tp is the buoy peak wave period. The orthogonal regression parameters (Table 1) illustrate the improvement, and we can verify that the NN-2 model enables significant reduction of the scatter between the altimeter and buoy measurements (see the distance parameter). The correlation coefficients between the buoy and altimeter wave period measurements for the global dataset are 0.78, 0.88, and 0.91 for the SOC, the NN-1, and the NN-2 models, respectively (Table 2). The associated standard deviations are 1.05, 0.81, and 0.7, respectively. Results in Table 2 are

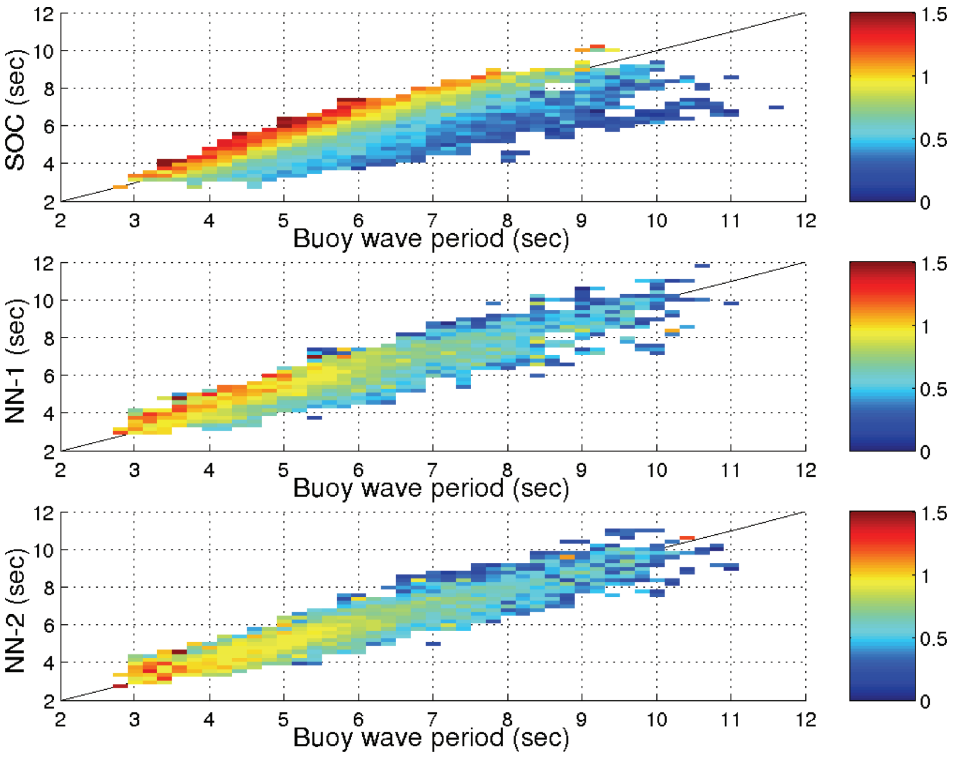

FIGURE 1 Comparisons of altimeter wave period models with the NDBC buoy wave period, color-coded as a function of the inverse wave age.

TABLE 1 Parameters of the Orthogonal Regression between the Buoy Wave Period and the Southampton Oceanographic Center Model (SOC), and the Two Neural Models NN-1 and NN-2 (Computations are Done for the Global Data-Set—(5904 Points.)

Model	SOC	NN-1	NN-2
Slope	1.17	0.99	1.03
Intercept (sec)	−0.48	0.01	−0.18
Distance (sec)	0.71	0.57	0.49

also given for data subsets corresponding to the buoys moored in the Hawai and Gulf of Mexico areas, because different swell conditions are usually encountered. It appears that the SOC model performance is very sensitive to regional sea surface degree of development and residual sea conditions, as already shown in Figure 1. This is further highlighted in Table 3 which reports the correlation coefficient of the models residuals (altimeter minus buoy wave period data) with the wind speed and the inverse wave age. These coefficients are computed for the global dataset and again for subsets corresponding to the buoys moored in the Hawai and Gulf of Mexico regions. These results provide further insight that the SOC and NN-1 models are more dependent on the wave age than on the wind speed solely, and that the SOC model residuals can be largely explained by its dependency on the wave age. This is still better observed in the Hawai area where the SOC correlation coefficient is above 0.8. Gommenginger et al. (2003) already reported that their model was less accurate in that region due to the presence of swell. We can also note in Table 3 that the NN-1 residuals are also significantly correlated, at 95% confidence level, with the wave age parameter, while this correlation vanishes nearly completely with the NN-2 model.

Figures 2a and 2b present the models biases as a function of the buoy wind speed and difference in C and Ku band backscatter coefficients, respectively. Indeed, the wind speed and the C band backscatter coefficient are the additional parameters used to define the NN-2 model. The results clearly indicate a large improvement with the NN-2 model compared to the others models. Figure 2c displays the models biases as a function of the buoy mean wave period. The SOC model produces large biases in the high wave period range, and the NN-1 model performs a little better than NN-2 in that range.

On Figure 3 are displayed histograms of the buoy and T/P altimeter NN-2 wave period measurements for the global dataset and for the specific areas covered by the NDBC buoy

TABLE 2 Statistical Comparisons between the Buoy Wave Period and the Southampton Oceanographic Center model (SOC), and the Two Neural Models NN-1 and NN-2 (for Each Model, Computations are Done for the Global Data-Set—Left, 5904 Points, the Hawai Area—Midde, 693 Points, and the Gulf of Mexico Area—Right, 1370 Points.)

Model	SOC			NN-1			NN-2		
Correlation	0.78	0.59	0.78	0.88	0.83	0.82	0.91	0.87	0.82
Bias (model–buoy, sec)	−0.5	−0.28	−0.2	0.03	0.23	0.08	−0.02	0.16	0.06
Std deviation (sec)	1.05	0.9	0.64	0.81	0.63	0.53	0.7	0.54	0.51

TABLE 3 Correlation Coefficient of the Models Residuals (Model Minus Buoy Wave Period) with the Buoy Wind Speed and Inverse Wave Age (The Considered Models are the Southampton Oceanographic Center Model (SOC), and the Two Neural Models NN-1 and NN-2. For Each Model, Computations are Done for the Global Data-Set—left, 5904 Points, the Hawai Area—Middle, 693 Points, and the Gulf of Mexico Area—Right, 1370 Points.)

Model		SOC			NN-1			NN-2	
Wind Speed	0.6	0.71	0.67	0.06	0.2	0.15	0.02	0.03	0.11
Wave Age	0.71	0.82	0.7	0.17	0.32	0.22	0.09	0.11	0.04

network. The histogram features (maximum, shape and tail) are nicely reproduced with the NN-2 model. The histograms are relatively spread in the West Coast and Alaska Gulf regions, featuring variable local conditions and frequent mean wave periods greater than 10 s. These large mean wave periods correspond to high wind seas and long swells propagating across the Pacific ocean. At the opposite, the Mexico Gulf histogram is sharper with a lower peak value, and very few mean wave periods greater than 8 s are encountered, because long swells are unable to develop. In the Hawai region, the histogram is also sharp because of the steady trade winds and the peak value of 6 s corresponds to mixed wind seas and swell trains. As already shown in Table 2, there is a small bias of the altimeter wave period towards positive values in the Hawai region, but the correlation coefficient remains large (0.87) despite the small dynamic range.

Cross-Calibration of TOPEX/Poseidon and Jason-1 Measurements

The mean wave period models described above have been defined for the TOPEX altimeter to benefit from the 12 years of collocated TOPEX/buoy data for calibration purpose. The Jason-1 satellite was launched in late 2001 and its altimeter presents the same instrumental characteristics as the TOPEX ones. It is thus possible to use the T/P wave period model for the Jason-1 altimeter after verification of the consistency of its measurements of significant wave height and radar cross-sections with the TOPEX ones. Using data from the Jason-1 and TOPEX/Poseidon tandem mission time period, it has been shown that there is a small Hs-dependent correction to apply to the Jason-1 Hs (P. Queffeulou, personal communication) and mean corrections to apply to the Jason-1 NRCS measurements (J. Dorandeu, personal communication). These mean corrections are slightly dependent on the altimeters cycle number, but are accurate enough to the first order. In this study, we have computed the bias corrections over January 2003, and we have verified the consistency with those referenced above. We have corrected the Jason-1 data to fit the TOPEX/Poseidon ones, by substracting 2.30 dB and 0.52 dB from the Ku and C band Jason-1 measurements, respectively. For information, the mean values proposed by J. Dorandeu are about 2.40 and 0.60 for the Ku and C band, respectively. Since the Hs distributions are nearly identical, we have only corrected the Jason-1 measurements for a small bias of 8 centimeters.

Using January 2003 T/P data and the adjusted Jason-1 data, we have computed the altimeters wave period estimates with the same neural model NN-2. The distributions are shown in Figure 4 and are found to be in excellent agreement. The small difference, if significant, can be attributed to the different ground sampling between Jason-1 and T/P.

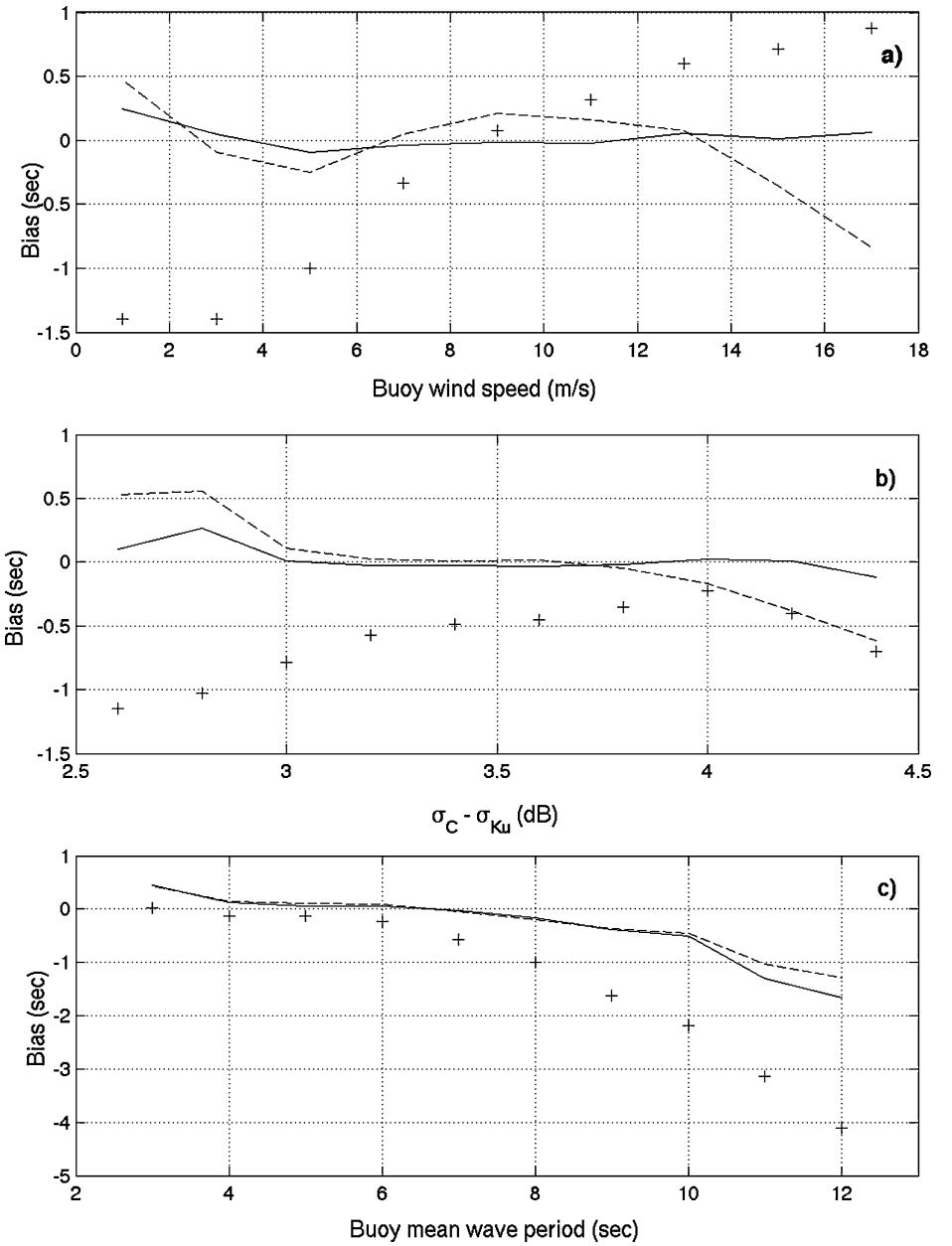

FIGURE 2 Mean wave period bias (altimeter minus buoy) as a function of: (a) the buoy wind speed; (b) the difference in the C and Ku bands normalized cross-sections; and (c) the buoy mean wave period. The altimeter wave period models are NN-2 (solid line), NN-1 (dashed line), and SOC (crosses).

Global Mapping of the Wave Period

Mapping Methodology

Since T/P and Jason-1 orbits are shifted to cover more efficiently, the sea surface in the tandem mission the space/time sampling is different for each altimeter. This fact, combined

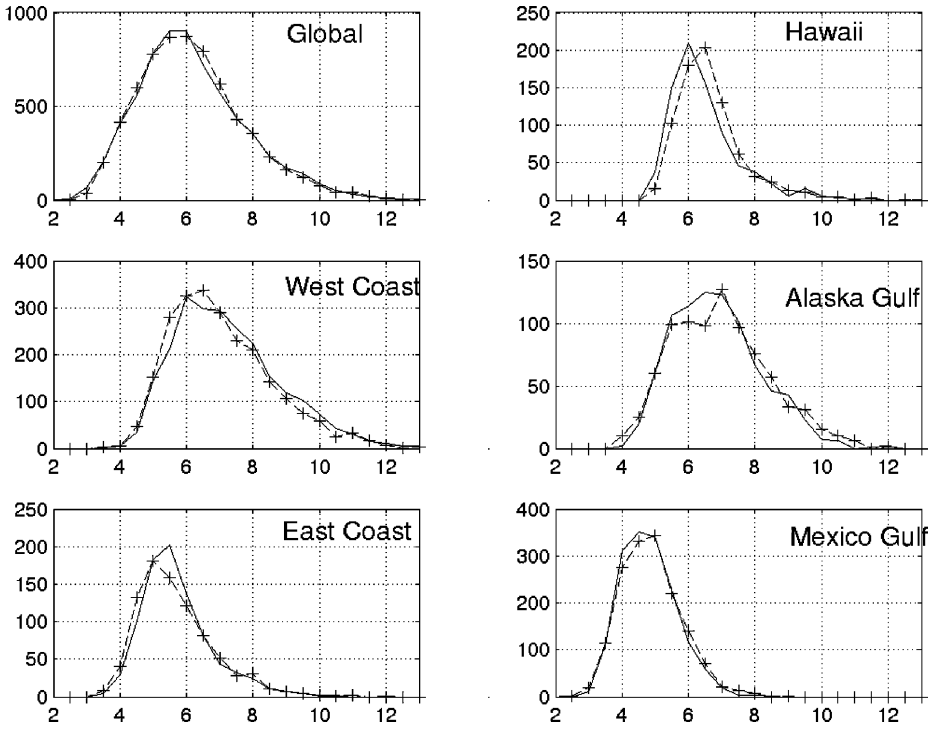

FIGURE 3 Distribution of buoy (solid line) and altimeter (dashed line) wave period measurements (sec) for the different areas covered by NDBC buoys.

with the relatively poor ground sampling of a highly variable parameter, such as the wave period by a nadir altimeter, make challenging the comparison of maps derived from the two altimeters. To minimize impacts of such sampling, we use the powerful Bayesian Maximum Entropy (BME) theory of modern spatiotemporal geostatistics (Christakos 2000; Serre et al. 2004), provided through the BMElib software package, to obtain maps showing the distribution of the physical variable across space and time. This theory provides a mathematically rigorous framework to integrate a wide variety of knowledge that belongs to two major bases: the general knowledge base (or soft data) that characterizes the variability of the process over space and time (physical laws, empirical relations, statistical moments of any order, scientific theories etc.), and the site-specific knowledge base (or hard data) that includes all the measurements of the process at specific space time points (measurements along the satellite path, uncertain observations, secondary information etc.) In this study, we have used the hard data solely (the T/P and Jason-1 measurements), as done in the classical space/time kriging approach. The advantage of using BMElib is that future works may naturally consider soft data (such as to provide characterization of local noise or information on the variable probability distribution function), leading to improved mapping results as shown in several BME studies (Serre et al. 2004). A more complete description of the method is given in the appendix.

Results

The mean wave period fields computed for T/P cycle 280 and Jason-1 cycle 37, corresponding to January 2003, on a 4° in longitude by 2° in latitude grid, are displayed in Figure 5.

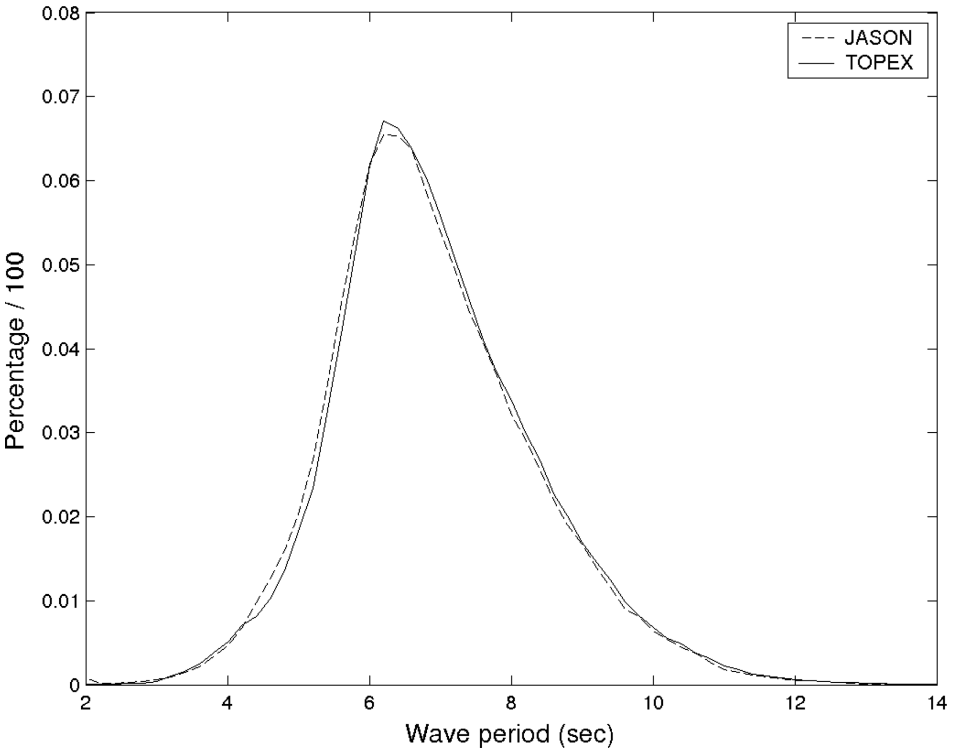

FIGURE 4 Distribution of the Jason-1 (solid lines) and TOPEX (dashed line) altimeter wave period for January 2003.

The geographical area is limited for better reading of the smaller structures, but the area is sufficiently extended to cover a large range of wave period and sea state conditions. As shown in Figures 5a and 5b, the large scale structures for the T/P and Jason-1 fields are in excellent agreement, and the smaller scale features are also delineated with a good confidence, since they are most of time reproduced on both maps. This indicates the overall consistency between T/P and Jason-1. Differences in the retrieved wave period maps are displayed Figure 5c. This shows differences lower than 1 s that appear to be mainly associated with differences in the location of the smallest scale structures. It is not surprising, given the relatively poor altimeter sampling, even if we use a robust interpolation method.

The orbital characteristics of the T/P and Jason-1 satellites are defined to provide in the tandem mission a better coverage and the above maps can be used to assess the interest of merging the two altimeter measurements to improve the retrieved wave period fields. This is illustrated in Figure 5d, which presents the mean dual-altimeter wave period field for the same analyzed time period.

Comparison with the WaveWatch-III Numerical Model

The previous section illustrates the ability of the altimeter measurements to map the mean wave period at local and global scales. Usefulness of these measurements is further illustrated in this section by comparing the altimeter mean wave period measurements to the values obtained with the WaveWatch-III (WW3) numerical wave model. WW3 (Tolman et al. 2002) is a third generation wave model developed at NOAA/NCEP in the spirit of the WAM model (WAMDIG 1988). For this study, the WW3 surface waves

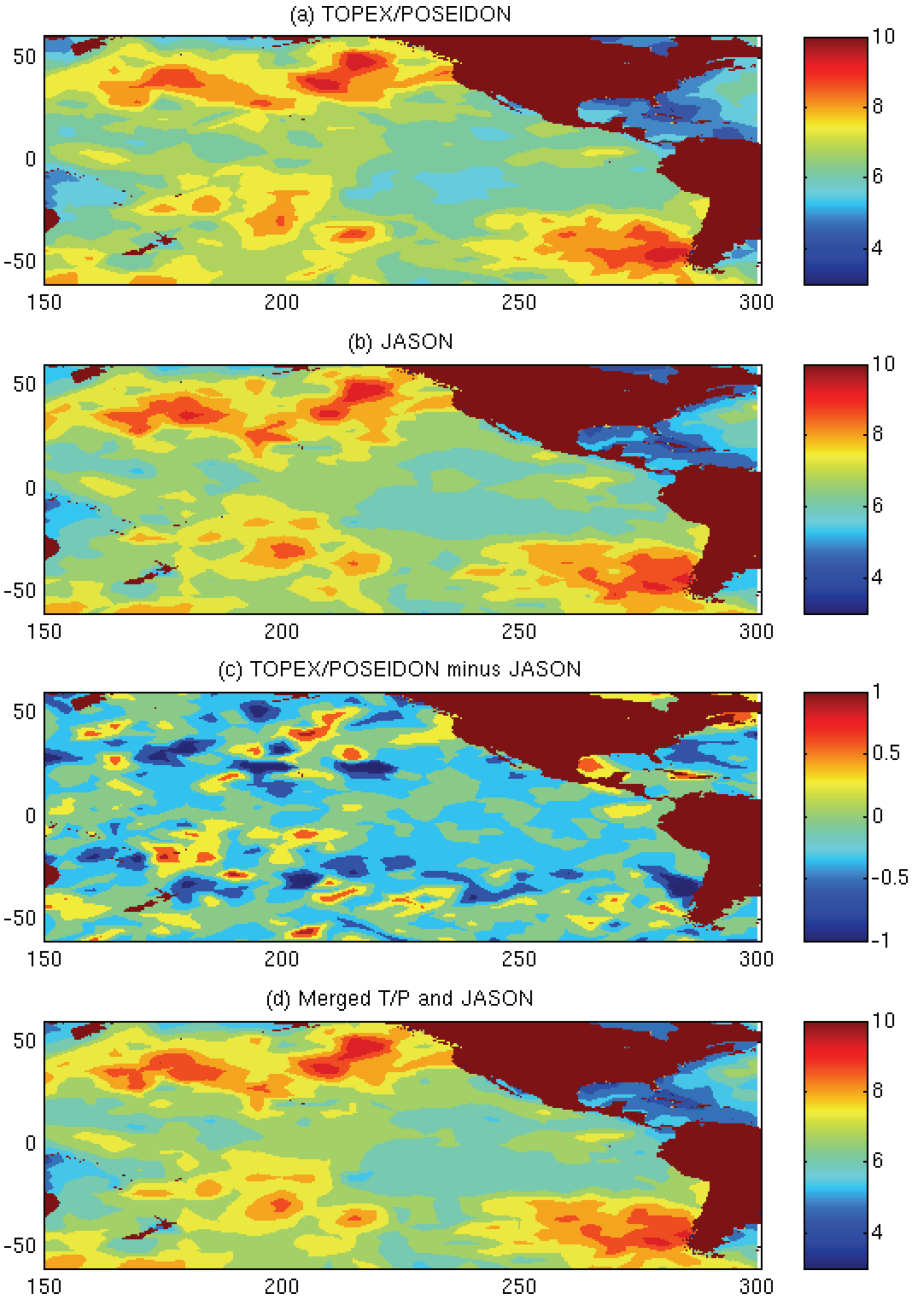

FIGURE 5 Mean altimeter wave period fields computed with T/P (a), Jason-1 (b), the mean difference (c), and the field from merged T/P and Jason-1 data (d), January 2003. All units are in seconds.

spectrum has been computed at global scale for January 2003 over a one degree resolution grid. The model time step is 15 minutes. The input wind field is a product merging measurements of the QuikScat scatterometer and the data from the NCEP numerical model (Chin et al. 1998). Its spatial and temporal resolutions are 0.5 degree and 6 hours.

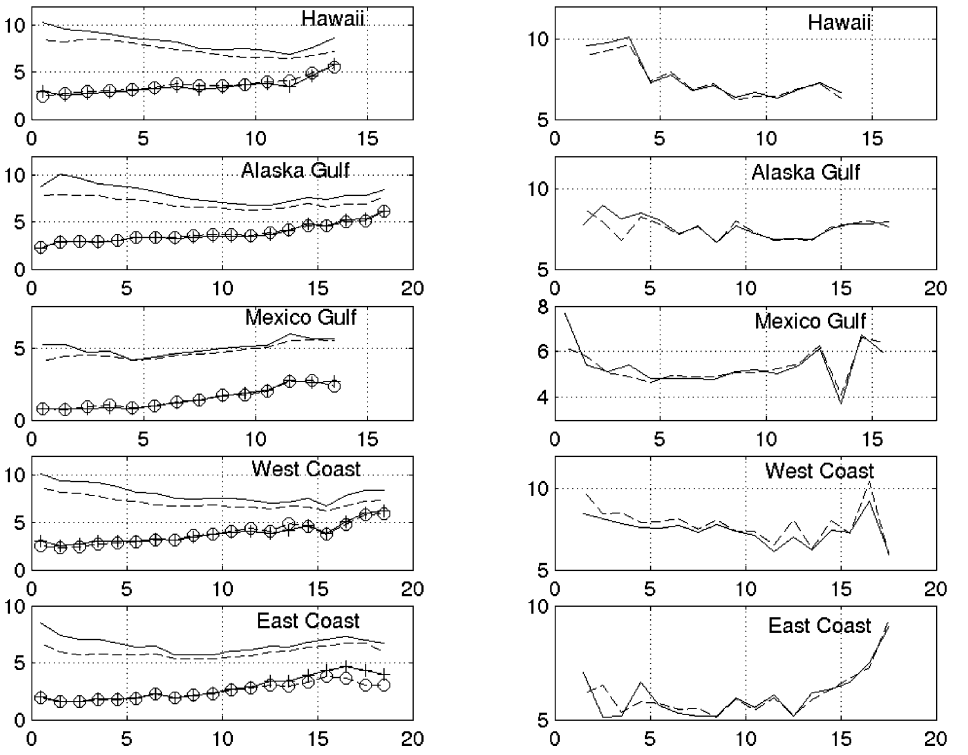

FIGURE 6 Mean altimeter (solid line, right and left panels), NDBC buoy (dashed line, right panel), and WW3 (dashed line, left panel) wave period (sec) as a function of the altimeter wind speed (m/s), for the different areas covered by NDBC buoys. Mean wave heights (m) are displayed on left panel for the altimeter (plus) and the WW3 numerical model (circles). The measurements cover January 2003 (left panel) and the January months for the time period 1992–2002 (right panel).

WW3 data have been interpolated at T/P and Jason-1 altimeters locations to produce the collocated dataset used in the following analysis. The obtained dataset has been divided into subsets corresponding to the main NDBC buoy regions. Figure 6 (left panels) presents, for these regions and for January 2003, the comparison between the altimeter and the WW3 mean wave periods and significant heights, as a function of the altimeter wind speed. Figure 6 (right panels) presents, for reference and for further altimeter mean wave period validation, the comparison between the altimeter and the NDBC buoy mean wave periods as a function of the altimeter wind speed. These latter curves have been obtained using the January months, 1992–2002, in order to be comparable with the altimeter/WW3 analysis with a good confidence. The obtained curves (right panels) confirm the excellent agreement between NDBC buoy and altimeter data. The comparison with WW3 indicates underestimation of the WW3 mean wave period over the whole wind speed range, with the exception of the Mexico Gulf. The long swells cannot develop in this region and the wave climate is thus dominated by the wind seas. This feature and the systematic WW3 mean wave period underestimation at low wind speed may indicate that the numerical model underestimates systematically the swell part of the wave spectrum. On the other hand, Figure 6 (left panels) shows an excellent agreement between the WW3 and altimeter significant wave heights, suggesting that the wind forcing is adequate. Underestimation of the WW3 mean wave period may be attributed to the wave model physics or parameterizations, and the altimeter

mean wave period can thus be used as an interesting additional parameter for numerical model tuning and physics understanding.

Conclusions

Sea state conditions directly impact altimeter radar cross section measurements. The importance of including sea state parameters in model inversion (altimeter wind, sea state bias) is still open, but is undoubtedly necessary when trying to retrieve mean wave period parameters from these combined altimeter measurements. Compared to previous attempts, this study benefits from a larger number of high quality collocated data accumulated along the T/P mission. While the impact of various sea state parameters (wave age, wave height, significant slope, etc.) has been already identified and thoroughly studied from field experiments, simplified parametric models do not exist and neural networks methodology appears well suited. The high quality data-set further helps to derive robust and practical empirical models. The altimeter mean wave period measurements, obtained from the NN-2 neural model presented in this study, is in excellent agreement with the NDBC buoy measurements. A large improvement is obtained by comparison with others altimeter empirical models, especially because the NN-2 model does not present systematic biases as a function of the sea state degree of development. The neural network methodology has thus proved to be efficient to derive an empirical model without addressing uncertain physical assumptions and parameterizations. The T/P and Jason-1 altimeter measurements have been cross-calibrated in order to provide coherent wave period estimates from the NN-2 model. The T/P and Jason-1 tandem mission is an opportunity to obtain enhanced space/time mean regular fields of the altimeter parameters (sea surface height, wind speed, wave height, etc.). A geostatistical method has been used to produce such regular mean fields to illustrate the interest of the altimeter wave period measurement to improve knowledge of the local and global sea state conditions. Furthermore, a comparison with the WaveWatch-III numerical wave model has been conducted to assess the altimeter wave period usefulness for wave model tuning and validation.

The obtained results are certainly encouraging and of interest in the pursuit of a better understanding of both wind sea growth and dissipation in the open ocean, and possible related sea state bias signatures. Thus they are interesting for satellite sensor physics understanding, as well as for the practical purpose to provide enhanced valuable information from altimeter data for engineering applications related to sea state and numerical modeling. Future works shall focus on better characterization of the mean wave period field as a function of the desired space/time resolution and altimeter inputs, and shall investigate the possible improvements to be obtained by adding specific constraints (altimeter measurement noise and wave period distribution characteristics, etc.) that can be specified in the BMElib interpolation method. Systematic comparison with the surface wave numerical models will further enable better understanding and interpretation of the obtained wave period fields and will address the topic of usefulness of altimeter wave period data assimilation.

References

Barrick, D. E. 1974. Wind dependence of quasi-specular microwave sea scatter. *IEEE Trans. Antenna Prop.* AP-22:135–136.

Chin, T. N., R. F. Milliff, and W. G. Large. 1998. Basin scale, high-wavenumber sea surface wind fields from a multiresolution analysis of scatterometer data. *J. Atmos. Ocean Tech.* 15:741–763.

Christakos, G. 2000. *Modern Spatiotemporal Geostatistics*. Oxford University Press, New York.

Davies, C. G., P. G. Challenor, and P. D. Cotton. 1997. Measurement of wave period from radar altimeters. *Ocean wave measurement and analysis*, pp. 819–826. edited by B. L. Edge, and J. M. Hemsley. Am. Soc. Civil Eng., Virginia, USA.

Fu, L.-L., and R. E. Glazman. 1991. The effect of the degree of development on the sea state bias in radar altimetry measurement. *J. Geophys. Res.* 96(C1):829–834.

Glazman, R. E., and S. H. Pilorz. 1990. Effects of sea maturity on satellite altimeter measurements. *J. Geophys. Res.* 95:2857–2870.

Gommenginger, C. P., M. A. Srokosz, P. G. Challenor, and P. D. Cotton. 2003. Measuring ocean wave period with satellite altimeters: A simple empirical model. *Geophys. Res. Lett.* 30(22):2150, 0.1029/2003GL017743.

Gourrion, J., D. Vandemark, S. A. Bailey, B. Chapron, C. P. Gommenginger, P. G. Challenor, and M. A. Srokosz. 2002a. A two parameter wind speed algorithm for Ku-band altimeters. *J. Atmos. Ocean Tech.* 19(12):2030–2048.

Gourrion, J., D. Vandemark, S. Bailey, B. Chapron. 2002b. Investigation of C-band altimeter cross section dependence on wind speed and sea state. *Canadian J. of Remote Sensing* 28(3):1–6.

Hornik, K., M. Stinchcombe, H. White. 1990. Multilayer Feedforward Networks are universal Approximators. *Neural Networks* 2:359–366.

Hwang, P. A., W. J. Teague, G. A. Jacobs, and D. W. Wang. 1998. A statistical comparison of wind speed, wave height and wave period derived from satellite altimeters and ocean buoys in the Gulf of Mexico region. *J. Geophys. Res.* 103:10451–10468.

Kitaigorodskii, S. A. 1973. The physics of air sea interaction. Israel Program for Scientific Translations.

Serre, M. L., G. Christakos, and S.-J. Lee. 2004. Soft data space/time mapping of coarse particulate matter annual arithmetic average over the U.S. In X. Sanchez-Vila and J. Carrera, eds. *Geostatistics for Environmental Applications*, Kluwer Academic Publishers, Dordrecht.

Tolman, H. L., B. Balasubramaniyan, L. D. Burroughs, D. V. Chalikov, Y. Y. Chao, H. S. Chen, and V. M. Gerald. 2002. Development and implementation of wind generated ocean surface wave models at NCEP. *Wea. Forecasting*, 17:311–333.

Tournadre, J., and J. C. Morland. 1997. The effect of rain on TOPEX/Poseidon altimeter data: A new rain flag based on Ku and C band backscatter coefficients. *IEEE Trans. Geosci. Remote Sens.* 35:1117–1135.

WAMDIG. 1988. The WAM model—A third generation ocean wave prediction model. *J. Phys. Oceanogr.* 18:1775–1810.

White, H. 1990. Connectionist nonparametric regression: Multilayer feedforward networks can learn arbitrary mappings. *Neural Networks* 3:535–549.

Appendix

The BME framework uses the theory of Space/Time Random Fields (S/TRF) to characterize the randomness of the process $X(\boldsymbol{s},t)$ over space $\boldsymbol{s}$ and time t on the basis of the general knowledge $\mathcal{G}$, and it uses a Bayesian conditionalization rule to process the site-specific knowledge $\mathcal{S}$ and produce a posterior pdf of $X(\boldsymbol{s},t)$. This posterior pdf varies across space and time and provides a complete stochastic description of the physical variable at any mapping point. In general the BME posterior pdf is not limited to the Gaussian form. However in this work, we limit the general knowledge base $\mathcal{G}$ considered to only include the mean trend $m_X(\boldsymbol{p}) = \mathrm{E}[X(\boldsymbol{p})]$ and space/time covariance $c_X(\mathrm{p},\boldsymbol{p}') = \mathrm{E}[(X(\boldsymbol{p}) - m_X(\boldsymbol{p}))\,(X(\boldsymbol{p}') - m_X(\boldsymbol{p}'))]$ of the S/TRF $X(\boldsymbol{s}, t)$, where $\boldsymbol{p} = (s, t)$ and E denotes stochastic expectation. We also limit the site specific knowledge $\mathcal{S}$ to consist only of hard data (exact measurements). In this limiting case, the BME posterior pdf is Gaussian with the same posterior mean and variance as that of kriging. This illustrates the generalization power of BME. The well-known space/time kriging method is obtained as a limiting case when only hard data is used.

In order to apply the *BMElib* space/time kriging approach to our problem, we had first to model the space/time covariance of the Space/Time Random Fields (S/TRF) $X(\boldsymbol{s}, t)$, and then use that covariance model together with the space/time satellite data to calculate the

kriging estimates at the nodes of a mapping grip. The covariance function obtained using *BMElib* was a nonseparable space/time model with parameters varying depending on the spatial and temporal region considered. This covariance model provides *BMElib* with a space/time metric allowing the selection of a local neighborhood of space/time satellite data that are closest to the space/time mapping point considered. A challenging aspect of our dataset was the massive amount of data collected along each path of the satellite. This issue was effectively addressed in our work by using, in addition to the local neighborhood of the data points closest to the mapping point, a second neighborhood of data points chosen to consider points over a wider space/time region.